Detailed prediction of fluid-solid coupled phenomena of turbulent flow through reed valves

IOP Conf. Series: Materials Science and Engineering **604** (2019) 012064 doi:10.1088/1757-899X/604/1/012064

Detailed prediction of fluid-solid coupled phenomena of turbulent flow through reed valves

I González, A Naseri, J Rigola, C D Pérez-Segarra and A Oliva

Heat and Mass Transfer Technological Center (CTTC), Universitat Politècnica de Catalunya - BarcelonaTech (UPC), ESEIAAT, Colom 11, 08222, Terrassa (Barcelona), Spain

E-mail: cttc@cttc.upc.edu

Abstract. The operation of self-actuated valves in suction and discharge processes plays a crucial role in the thermal efficiency and structural reliability of hermetic reciprocating compressors. The present work provides a thorough description of an in-house numerical method based on a partitioned fluid-structure interaction algorithm intended to obtain high-fidelity numerical predictions and optimise valve system design. A large eddy simulation model is used for the turbulent flow, whereas a normal mode superposition assumption along with an impact penalty method is used for the reed. Under this framework, a detailed analysis of the coupled problem with a straight and tapered exit ports is carried out. Differences in effective flow area and pressure drop are found as a result of the port geometry, but also of the valve velocity.

1. Introduction

Reed valves are used to control suction and discharge processes of hermetic reciprocating compressors. The significance of their design lies in the great influence they have on the efficiency, structural reliability and sound radiation of the compressor [1, 2, 3]. Almost half of the thermodynamic losses of the device relate to valve operation [4], whereas the fatigue from valve impact and bending is the most common cause of failure of the compressors [5, 6].

The problem involves a fluid-structure interaction (FSI) phenomenon since the valves are self-activated as a result of a pressure difference. Traditionally the coupled process has been studied with one-dimensional lumped models, which are suitable for broad design studies [1, 7]. However, further optimisation of the system requires obtaining a better understanding of the physics that develops (pressure losses, flow topology and turbulent effects, backflow, fluttering, collisions, etc.), by means of high-fidelity models.

Several recent works in the literature combine a 3D computational fluid-dynamic simulation (CFD) with the dynamic deformation of the valve. For instance, in [8, 9, 10], a validation of FSI computational methods was carried out by reproducing experimental results of reed valves. Furthermore, the FSI numerical prediction has allowed investigating the effect of gas velocity [11], valve thickness [12] and other geometrical parameters [13, 14] on the process efficiency. Most authors used commercial software and focused on the structural solution, rather than describing thoroughly the numerical procedure or studying also the flow behaviour.

This work aims at presenting a finite volume method to be included in the design process of industrial applications with FSI and demonstrating its validity to analyse the turbulent flow through self-actuated valves. The method is based on an FSI partitioned algorithm to strongly

couple a CFD simulation with LES turbulence modelling to a plate model for the valve. The numerical analysis focus on the dynamic response of the system using different geometries of the outflow port.

First, the numerical methodology is fully described in section 2. Next, section 3 define the specific case parameters, whereas section 4 summarises the obtained results.

2. Numerical method

A partitioned approach is followed to solve the FSI problem, which uses independent solvers for fluid and structural sub-problems and adopts a coupling scheme to account for their interaction. The elastic reed motion is modelled using the normal mode summation method, within a Lagrangian mesh, thus taking the local loads and bending deformations into account with negligible computational effort. On the other hand, the fluid flow is solved with a parallel CFD code on a 3D unstructured grid which automatically adapts to the dynamic boundaries defined by the solid motion.

2.1. Fluid model

Fluid flow is assumed isothermal and incompressible, hence the modelisation with Navier-Stokes equations. Integrating over a moving control volume V leads to an arbitrary Lagrangian-Eulerian (ALE) formulation of the conservation equations of mass, momentum, and space:

$$\int_V \nabla \cdot \dot{\boldsymbol{u}} dV = 0\,, \tag{1}$$

$$\frac{\partial}{\partial t}\int_V \rho \dot{\boldsymbol{u}} dV + \int_V \rho \dot{\boldsymbol{c}} \cdot \nabla \dot{\boldsymbol{u}} dV = \int_V \nabla \cdot \boldsymbol{\sigma} dV\,, \tag{2}$$

$$\frac{\partial}{\partial t}\int_V dV - \int_S \boldsymbol{n} \cdot \dot{\boldsymbol{u}}_g dS = 0 \tag{3}$$

where ρ is the density, p is the pressure, $\dot{\boldsymbol{u}}$ is the fluid velocity, and $\dot{\boldsymbol{c}}$ is the total convective velocity, which depends on the fluid velocity and the velocity of the moving reference $\dot{\boldsymbol{u}}_g$ as $\dot{\boldsymbol{c}} = \dot{\boldsymbol{u}} - \dot{\boldsymbol{u}}_g$. The stress tensor $\boldsymbol{\sigma}$ is defined by the constitutive equation of a Newtonian fluid as:

$$\boldsymbol{\sigma} = -p\boldsymbol{I} + \mu\left[\nabla \dot{\boldsymbol{u}} + (\nabla \dot{\boldsymbol{u}})^T\right]\,, \tag{4}$$

where μ is the dynamic viscosity of the fluid. Applying the constitutive model and the divergence theorem to equation 2 yields the following form of the momentum conservation law

$$\frac{\partial}{\partial t}\int_V \rho \dot{\boldsymbol{u}} dV + \int_S \dot{\boldsymbol{u}}\left(\rho \dot{\boldsymbol{c}} \cdot \boldsymbol{n}\right) dS = \int_S \mu \boldsymbol{n} \cdot \nabla \dot{\boldsymbol{u}} dS - \int_S p \cdot \boldsymbol{n} dS\,. \tag{5}$$

A finite volume method is used to solve the governing equations. Second-order symmetry-preserving schemes are followed to discretise the equations on a collocated unstructured grid arrangement. These schemes guarantee the conservation of kinetic energy in the discrete representation, a crucial feature when dealing with turbulent flows [15].

An explicit time integration discretises the convective and diffusive terms of the momentum equation, whereas an implicit scheme is used for the pressure gradient term. The fractional-step projection method is intended for decoupling and solving pressure and velocity with a three-step solution procedure.

Special attention should be paid to the evaluation of the grid velocities $\dot{\boldsymbol{u}}_g$ in order to satisfy the space conservation law (equation 3) and thus avoid numerical errors in the form of artificial mass sources [16]. The discretised counterpart of equation 3, should share the same numerical

schemes employed for Navier-Stokes equations. An exact computation of the volume swept by each face of the control volume is used to evaluate the volume difference.

Large Eddy Simulation (LES) models are used for turbulence. In LES, the largest scales of the flow are solved while the small-scale motions are emulated by a subgrid-scale model, reducing the computational cost of direct numerical simulations. Navier-Stokes equations are filtered spatially, and a modelisation is required for the filtered non-linear convective term. To do so, a subgrid-scale stress tensor is formulated as a function of a subgrid-scale viscosity ν_{sgs}. In this work, such viscosity is calculated according to the wall-adapting eddy viscosity model [17].

2.2. Fluid mesh motion

The automatic deforming mesh method adjusts the position of the internal mesh points to accommodate changes in the domain boundary without involving topological alterations. In this case, it is the fluid mesh that has to be adapted to the motion of the structure. The method to be used provides the incremental displacement of the grid points between two consecutive time steps $\boldsymbol{u}_g$, by solving a pure diffusive problem. Therefore, a Laplace equation is written for each control volume volume:

$$\int_S D_g \boldsymbol{n} \cdot \nabla \boldsymbol{u}_g dS = 0\,. \tag{6}$$

The system of equations is determined by defining boundary conditions of Dirichlet type (moving or fixed boundaries) or Neumann (sliding or free boundaries). The diffusion coefficient D_g depends on the element volume according to

$$D_{g,i} = 1/V_i^{\chi}\,, \quad \chi \geqslant 0\,. \tag{7}$$

Consequently, the small cells, which are generally located at numerically or physically meaningful areas, become stiffer and harder to deform and the major distortion is absorbed by the softer large cells, which can readily tolerate the deformation without severely degrading their quality.

2.3. Plate model

The reed valve is considered as an arbitrarily shaped plate with uniform thickness h, where (x, y) are the coordinates on its mid-surface and z is the coordinate in the thickness direction. Such structure will be modelled by the isotropic Kirchhoff-Love plate theory, which is suitable for thin plates subjected to transverse loads t_z and small strains and rotations. After applying the kinematics assumptions, the problem becomes two-dimensional in (x, y):

$$\frac{Eh^3}{12\left(1-\nu^2\right)}\nabla^4 u_z\left(x,y,t\right) + 2\rho h \ddot{u}_z\left(x,y,t\right) = t_z\left(x,y,t\right)\,, \tag{8}$$

where u_z is the normal displacement.

In order to reduce the computational cost of a direct time integration, the mode superposition method for linear analysis is followed. Thus, the motion of a vibration system can be approximated by a combination of a limited number M of its free vibration modes [18]:

$$u_z\left(x,y,t\right) \approx \sum_{m=1}^{M} q_m\left(t\right)\phi_m\left(x,y\right)\,, \tag{9}$$

where $\phi_m\left(x,y\right)$ and q_m are the normal deformation pattern and the generalised coordinate corresponding to the vibration mode m, respectively. Mode shapes $\phi_m\left(x,y\right)$ and natural radial frequencies ω_m have to be obtained beforehand by solving the eigenvalue problem of the free

vibration equation of the system. Imposing the mode superposition to equation 8 and considering their orthogonality ($\int_S \phi_m \phi_n dS = 0$ if $m \neq n$) transform the original continuum equation into a set of M independent equations, one for each mode, written in terms of the generalised coordinates [3]:

$$\ddot{q}_m(t) + \omega_m^2 q_m(t) = \frac{\int_S \phi_m(x,y) t_z(x,y,t) dS}{\rho h \int_S \phi_m^2(x,y) dS} \,. \tag{10}$$

Three different sources can cause transverse load in the reed system: fluid pressure and shear stress $\boldsymbol{n} \cdot \boldsymbol{\sigma}$ (equation 4), gravitational force $\boldsymbol{g}$ and impact force with the seat I, considered totally perpendicular. If $\boldsymbol{n}$ is the unit normal outward to the plate in the current configuration, the transverse load results in:

$$t_z\left(x,y,t\right) = (0,0,1) \cdot \left[\boldsymbol{n}\left(x,y,t\right) \cdot \boldsymbol{\sigma}\left(x,y,t\right) + \rho \boldsymbol{g} h\right] + \frac{I\left(x,y,t\right)}{dS} \,. \tag{11}$$

Any other force, such as reed pre-tension or stiction force, is omitted at this stage. Thus, the total energy of the valve, which is the sum of kinetic energy e_T, strain energy e_K and gravitational potential energy e_G, should balance the work done by fluid and impact forces.

The numerical resolution of the system of M equations 10 is conducted by an integration over both upper and bottom surfaces of the valve plate. Once the load t_z on the face elements of the structure is known, the midpoint rule is used to approximate the right-hand side of equations 10. Then, a trapezoidal rule discretises in time the remaining terms and q_m solutions can be found.

The penalty method models the frictionless contact with the rigid seat. When a valve element penetrates the seat, a local impact force proportional to this penetration δ_i is recalled:

$$I_i = \begin{cases} \kappa_i \delta_i & \text{if } \delta_i > 0 \\ 0 & \text{if } \delta_i \leqslant 0 \,, \end{cases} \tag{12}$$

where κ_i is the penalty stiffness. The higher the stiffness, the better the accuracy (less penetration), but the more numerically unstable. In this case, it is sized according to [19] recommendation:

$$\kappa_i = f_{SI} \frac{K S_i^2}{S_i h} \,, \tag{13}$$

where K is the plate bulk modulus and f_{SI} is a scale factor which has been set here to 1, thanks to the small time steps employed. Like the fluid pressure force, the impact force is integrated implicitly in the equilibrium equation and thus, an iterative process is required.

2.4. Fluid-solid coupling algorithm

Kinematic and dynamic equilibrium should be satisfied on the fluid-solid interface. In the partitioned approach, equal velocities are imposed on the fluid boundary condition as

$$\dot{\boldsymbol{u}}_f = \frac{\partial \boldsymbol{u}_s}{\partial t} \,, \tag{14}$$

whereas equal stresses are imposed on the solid boundary condition as

$$\boldsymbol{n} \cdot \boldsymbol{\sigma}_s = \boldsymbol{n} \cdot \boldsymbol{\sigma}_f = \boldsymbol{t}_f \,, \tag{15}$$

where $\boldsymbol{n}$ is the unit normal vector at the interface.

An implicit partitioned coupled system needs to solve the coupled fluid-solid system by an iterative process. Despite the numerical stability shown by implicit methods, they are

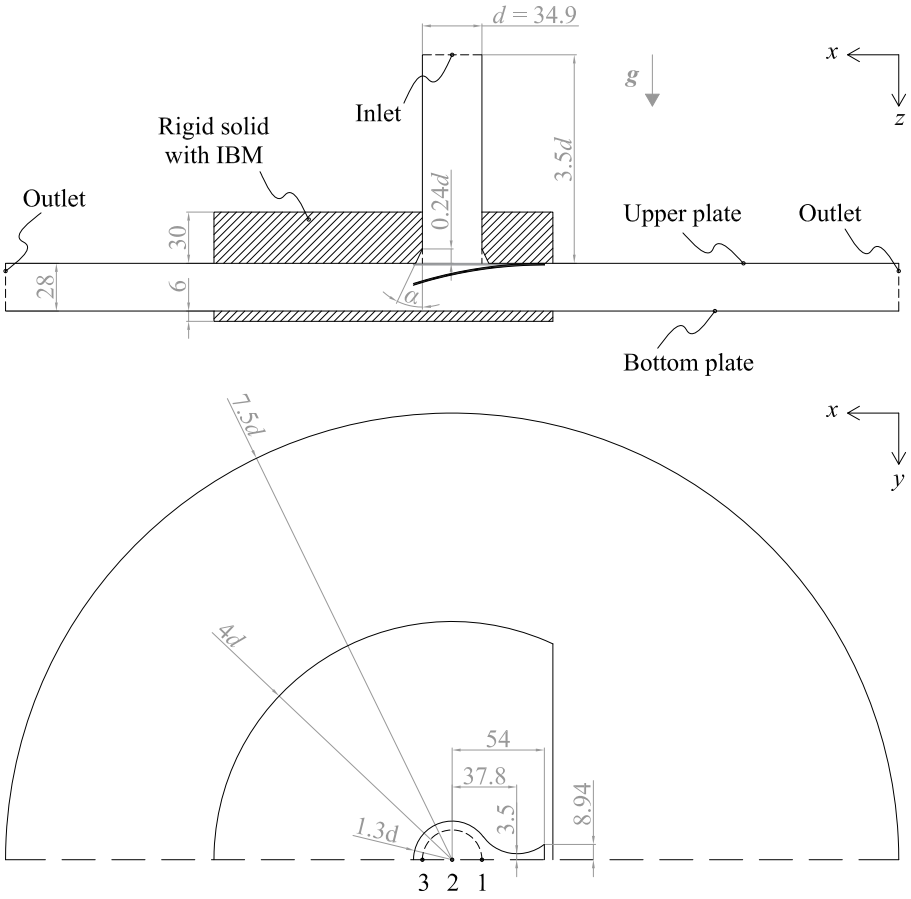

Figure 1. Two views of the computational domain with dimensions in mm. Control point 2 for lift measurements.

computationally expensive because fluid and solid equations should be solved several times at every time step. To alleviate this, here a semi-implicit approach to handle strongly coupled problems is employed. It leverages the fluid projection method to implicitly couple only the pressure term to the structure, without moving the mesh nor correcting the velocities at every fluid coupling iteration. Complete description of the fluid-solid algorithm can be found in [20].

3. Case definition

The test rig of [21], which measured the fluttering motion of a reed valve under the load of a developed and stationary air pipe flux, is followed here to define the reference case. The configuration resembles more of a suction valve, although some results could be extended to discharge valves too.

The numerical study aims at determining the effect of the channel port shape on the outflow performance of a self-acting valve. The assembly consists of a feeding tube with $d = 34.9$ mm in diameter, closed by the valve at the end, and a space between two plates downstream of the valve. The thickness of the valve is $h = 0.4$ mm and the diameter $D = 1.3d$. Following the work from [22] for a static configuration of a valve disk, two different angles will be tested for a tapered exit port with height $0.24d$: $\alpha = 0$ and $\alpha = 20^{\text{o}}$. Figure 1 shows all other dimensions of the valve as well as those of the computational domain chosen for the simulations. Inlet and outlet boundaries have been located sufficiently far from the valve to avoid their influence in the

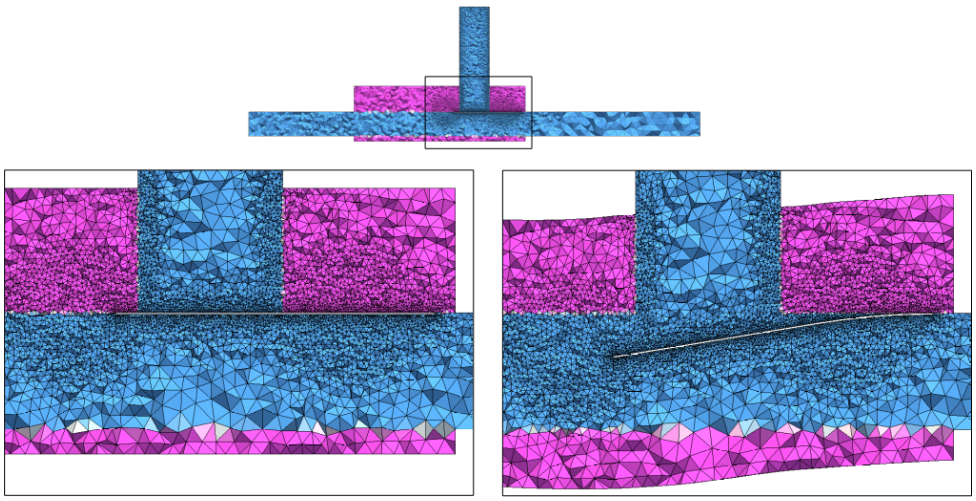

Figure 2. Mesh for the straight port at different instants. On the left when the reed valve is completely closed, and on the right when it is opened. Fluid elements in blue and immersed rigid body elements in pink.

solution.

The temperature of the air is 25 °C, ambient pressure is defined at the outlet, and gravity is $\boldsymbol{g} = (0, 0, 9.81)$ m/s^2. The physical properties of the flexible valve are set to be: $\rho = 7850$ kg/m^3, $\nu = 0.3$ and $E = 2 \cdot 10^{11}$ Pa. In this work, the inlet velocity of the fluid is determined such that Reynolds number is $10,000$:

$$Re = \frac{\rho \bar{u}_z d}{\mu}, \tag{16}$$

where $\bar{u}_z$ is the axial bulk velocity. The inlet velocity is fixed following the profile of a developed pipe flow. This averaged velocity profile has been approximated by that corresponding to a similar value of Re [23].

3.1. Numerical parameters

The generated fluid mesh defines an element size of 0.75 mm on both surfaces of the plate, 0.5 mm on the plate perimeter and 1.5 mm on the walls of the feeding pipe. A total of $2.2 \cdot 10^6$ tetrahedral control volumes is reached. The number of control volumes for the solid is $2.1 \cdot 10^4$.

This fluid mesh resolution resulted from a grid independence test, as a compromise between accuracy and computational cost. The current mesh showed 31 % difference in the valve deflection when compared to a mesh with double cell sizes, and 16 % when compared to a mesh with halved cell sizes. Despite the deviations, the trends in the coupled solution are equivalent and the present grid can be used to conduct a comparative study of the system.

Throughout valve opening, a gap will appear between the valve and the seat, making necessary a new set of fluid elements in that zone. In order to avoid a remeshing procedure, there will be moving elements which will perform as solid (upper plate) when valve is closed, and as fluid when it is opened. This change in the elements nature is achieved using an immersed boundary method (IBM) [24] and is shown in figure 2. Figure 1 includes the dimensions of the required auxiliary regions. As can be seen in both pictures, extra elements have been added as well at the bottom plate. They will help to accommodate the mesh deformation and to preserve mesh quality when the valve opens.

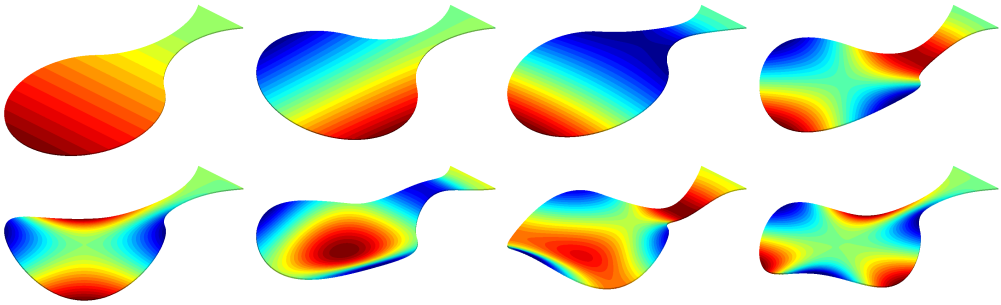

Figure 3. Deformation pattern of the first eight free vibration modes of the plate, ordered from left to right and from top to bottom. Colours according to the normal displacement. Associated natural frequencies in Hz: 30.6, 129.3, 319.7, 980.6, 1039.4, 1545.1, 2038.6, 2287.9

The size of the time step is automatically maximised ensuring numerical stability of the explicit fluid model according to the method described in [25].

4. Results and discussion

First, a modal analysis has been carried out with a commercial software to find the mode shapes ϕ_m and the radial frequencies ω_m of the free vibrating reed with clamped boundary condition in its root. Since the reed is subjected to impact with a rigid plate with an orifice, the study considers the first 15 normal modes of the structure [26]. The solution of the normal mode analysis is summarised in figure 3.

The solution of the entire transient FSI analysis is summarised in figure 4. At the beginning, the gas flow impacts with the closed valve, generating a pressure load that abruptly bends the valve and opens the flow passage (see time evolution of the lift). Although the first mode of vibration predominantly governs the deformation, higher modes are also excited because of the sudden fluid load. As can be seen in the first opening cycle, more than 95 % of the energy of the valve (kinetic, strain and gravitational potential) is gained, through a positive work of the fluid, when $s_2/d < 0.02$. At this moment, if no more gas would flow, the solid would conserve this gained total energy, by oscillating endlessly, since no structural damping has been considered within the plate model. Nevertheless, in this case, the steady incompressible flow is working as a viscous damper of the solid vibration.

As the reed starts closing and flow passage narrows, pressure upstream soars to ensure that the entire mass of incoming fluid can be evacuated from the channel and thus satisfy the continuity law. Such a pressure peak together with the fluid cushion placed between valve and seat is capable of stopping the reed before it collides with the seat. In this way, the solid with no speed is in an open position, resulting in a fluid force and work that are lower than those reached at the beginning, when the valve was stopped but completely closed. The total energy absorbed by the fluid diminishes, and so does the lift and the inertia to later approach the base.

Regarding the differences between the two types of exit port. The first point to note is the similarity between the resulting deformation and dynamics of the valve. As mentioned above, the motion of the structure is governed by the peak of fluid force which develops when the flow passage is practically closed. Precisely, with this limited opening, the change of flow momentum is the same and the net force exerted and energy gained of the valve is equivalent in both cases. Thus, both result in a maximum lift at control point 1 of $s_1/d = 0.11$ ($s_2/d = 0.20$, $s_3/d = 0.30$) and an oscillation frequency of approximately 55 Hz.

The fundamental difference lies on the fluid side, namely in the pressure drop and flow topology. The time evolution of the pressure drop indicates that, except when the valve is

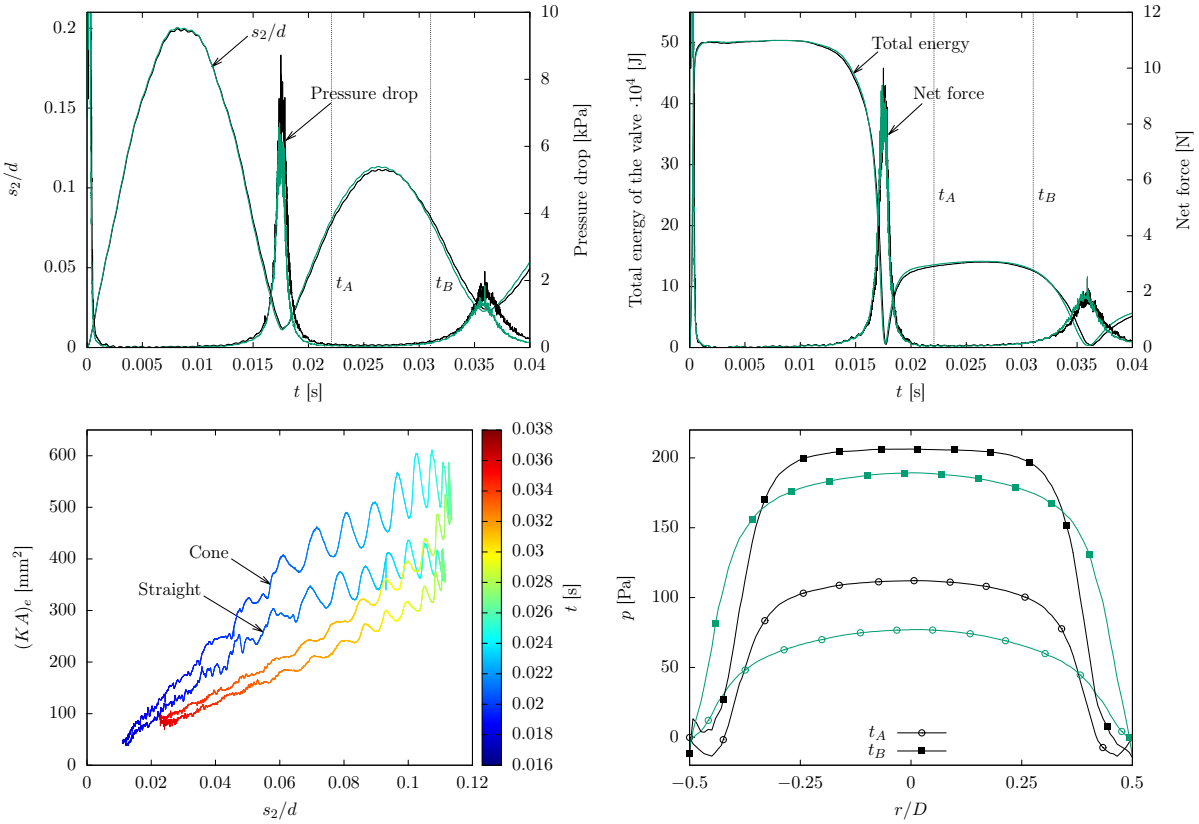

Figure 4. Clockwise from top left: lift at point 2 and pressure drop; energy and net force on the valve; relative pressure over the upstream face at $t_A = 0.022$ s (opening with $s_2/d = 0.08$) and $t_B = 0.031$ s (closing with $s_2/d = 0.08$); and effective flow area as a function of lift and time during the second opening cycle. Black lines correspond to the straight port while green lines to tapered port.

closed, the pressure required at the inlet is always lower with the tapered port. The cone orients and decreases the flow speed, and facilitates the gas evacuation through the radial diffuser. This means that the tapered shape of the port would improve the efficiency of suction/discharge processes. This property can also be measured via the effective flow area, which is calculated for incompressible flows as [3]

$$(KA)_e = \frac{\dot{m}}{\sqrt{2\rho(p_u - p_d)}}, \tag{17}$$

where pressure p_u is the upstream pressure (taken as the average pressure on the inlet boundary) and p_d is the discharge static pressure (taken as the pressure on the outlet boundaries). The value of this area as a function of valve lift and time during the second opening cycle is plotted in figure 4. On the one hand, again one can observe the greater difficulty to outflow with the straight port. The effective flow area is always smaller, although more pronounced as the valve separates. On the other hand, for the same port geometry, the effective area does not depend only on the reed lift but also on its velocity, since the area is larger when opening than when closing. This means that the pressure drop developed is higher when the valve wall moves against the pipe flow. Such velocity effect becomes perceptible because of the high frequency of the structure, which generates velocities of the same order as those of the fluid.

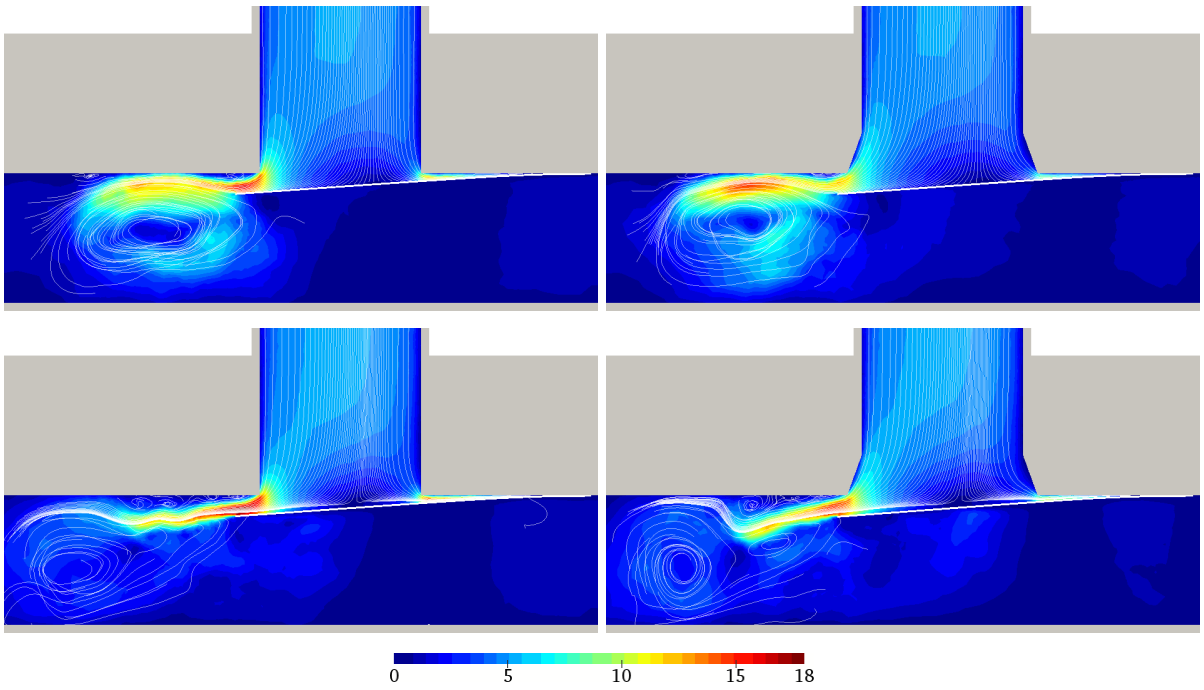

Figure 5. Velocity magnitude map (in m/s) and streamlines at t_A (top) and t_B (bottom). Straight port (left) and tapered port (right).

Two instants that share a common lift of $s_2/d = 0.08$ have been chosen to analyse how the fluid load and flow topology varies according to the mentioned sign of the reed velocity. See highlighted times $t_A = 0.022$ s (opening) and $t_B = 0.031$ s (closing) in figure 4. Pressure distribution over the upstream face of the valve at both instants is outlined in figure 4. The pressure is effectively higher when closing, due to the greater change of momentum of the colliding fluid particles. Given the reorientation of the flow with the tapered orifice, the obtained pressure profiles are wider and smoother.

Figure 5 shows the magnitude of the velocity at the same instants for both port geometries. At t_A the flow in the diffuser zone (between reed and seat) detaches from the valve and later reattaches to the seat, forming a recirculating bubble near the seat corner. Besides, a large vortex is developed around the valve perimeter. When the valve is closing at t_B, the mass flow through the diffuser rises, but the opening space is the same as in t_A. Therefore, velocity increases distorting the recirculating flow in the diffuser and the surrounding large-scale vortex.

5. Conclusions

A partitioned numerical method to solve dynamic problems with a strong interaction between a 3D turbulent flow and plate-type structures is presented. Its main features include: an ALE formulation with Laplacian mesh updating and LES turbulence modelling for the fluid, normal mode superposition with impact penalty method for the solid and a semi-implicit coupling algorithm for the interface problem. The method is used to simulate the coupled process of flow through self-activated valves. The numerical prediction is intended to compare the performance of suction/discharge processes obtained with two exit port shapes, one straight and one tapered. For a stationary inlet mass flow, the fluttering motion of the reed is the same for both alternatives. However, the conical port helps to orient the velocity field for a radial outflow and thus reduces the pressure drop of the process.

Acknowledgments
This work has been financially supported by the Ministerio de Economía, Industria y Competitividad, Spain (ENE2017-88697-R).

References
[1] Soedel W 1984 *Design and Mechanics of Compressor Valves* (Purdue University)
[2] Ferreira T S and Lainor J 1986 Analysis of the influence of valve geometric parameters on the effective flow and force areas *International Compressor Engineering Conference* (Indiana)
[3] Soedel W 1992 *Mechanics, Simulation and Design of Compressor Valves, Gas Passages and Pulsation Mufflers* (Purdue University)
[4] Ribas F A, Deschamps C J, Fagotti F, Morriesen A and Dutra T 2008 Thermal analysis of reciprocating compressors - A critical review *International Compressor Engineering Conference* (Indiana)
[5] Leonard S M 1996 *Hydrocarbon Processing* **75** 67 – 74
[6] Woo S, O'Neal D L and Pecht M 2010 *Engineering Failure Analysis* **17** 979 – 991
[7] Böswirth L 1996 A new valve dynamics simulation program and its use for the design of valves *International Compressor Engineering Conference* (Indiana)
[8] Mayer J, Bjerre P and Brune F 2014 A comparative study of different numerical models for flapper valve motion *International Compressor Engineering Conference* (Indiana)
[9] Parihar A, Myszka D, Robinet B and Hodapp T 2016 Integrating numerical models for efficient simulation of compressor valves *International Compressor Engineering Conference* (Indiana)
[10] Yu X, Tan Q, Ren Y, Jia X and Jin L 2017 *Energy Procedia* **105** 4890 – 4897
[11] Gasche J L, de Lima Dias A D S, Bueno D D and Lacerda J F 2016 Numerical simulation of a suction valve: Comparison between a 3D complete model and a 1D model *International Compressor Engineering Conference* (Indiana)
[12] Wu W, Jian Z, Song M and Zhang Z 2016 Study of valve motion in reciprocating refrigerator compressors based on the 3-D fluid-structure interaction model *International Compressor Engineering Conference* (Indiana)
[13] Coskun U C, Gunes H and Sarioglu K 2016 A numerical model of fluid structure interaction of a fluttering valve *Proceedings of the 5th International Conference on Jets, Wakes and Separated Flows (ICJWSF2015)* pp 421–429
[14] González I, Naseri A, Rigola J, Pérez-Segarra C D and Oliva A 2017 *IOP Conference Series: Materials Science and Engineering* **232** 012032
[15] Jofre L, Lehmkuhl O, Ventosa J, Trias F X and Oliva A 2014 *Numerical Heat Transfer, Part B: Fundamentals* **65** 53–79
[16] Demirdžić I and Perić M 1988 *International Journal for Numerical Methods in Fluids* **8** 1037–1050
[17] Nicoud F and Ducros F 1999 *Flow, Turbulence and Combustion* **62** 183–200
[18] Thomson W 1998 *Theory of Vibration with Applications (5th Edition)* (Taylor & Francis)
[19] Hallquist J O, Goudreau G L and Benson D J 1985 *Computer Methods in Applied Mechanics and Engineering* **51** 107 – 137
[20] Naseri A, Lehmkuhl O, Gonzalez I, Bartrons E, Pérez-Segarra C D and Oliva A 2018 *Journal of Fluids and Structures* **80** 94–112
[21] Gasche J L, Arantes D M and Andreotti T 2014 Experimental analysis of the fluid structure interaction in a suction valve model *International Compressor Engineering Conference* (Indiana)
[22] Rigola J, Aljure D, Lehmkuhl O, Pérez-Segarra C D and Oliva A 2015 *IOP Conference Series: Materials Science and Engineering* **90** 012026
[23] Kim J, Moin P and Moser R 1987 *Journal of fluid mechanics* **177** 133 – 166
[24] Favre F, Antepara O, Lehmkuhl O, Borrell R and Oliva A 2014 On the fast transient spoiler deployment in a NACA0012 profile using LES techniques combined with AMR and IMB methods *6th European Conference on Computational Fluid Dynamics (ECFD VI)* (Barcelona)
[25] Trias F X and Lehmkuhl O 2011 *Numerical Heat Transfer, Part B: Fundamentals* **60** 116–134
[26] Lo C C 1980 *Journal of Sound and Vibration* **69** 245 – 255